

Real-Time Nonlinear Transient Simulation Based on Optimized Transmission Line Modeling

Babak Asghari, *Student Member, IEEE*, and Venkata Dinavahi, *Senior Member, IEEE*

Abstract—This paper proposes an optimized transmission line modeling (TLM) method for the real-time transient simulation of systems with multiple nonlinearities. The proposed method allows the simulation to be carried out with larger time-steps while maintaining the accuracy. A detailed case study of a nonlinear bridge circuit is presented to illustrate the advantages of the optimized TLM method in comparison with other methods. The new formulation is then implemented in real-time for the transient simulation of the nonlinear bridge. Real-time simulation results are validated by comparing them with experimental measurements. A second case study includes a power system with several surge arresters which is also simulated in real-time by the aid of the optimized TLM method and verified using offline simulation.

Index Terms—Iterative methods, Newton-Raphson method, nonlinear circuits, power system transients, real-time systems, transmission line modeling.

I. INTRODUCTION

ELECTROMAGNETIC transient (EMT) simulation of power systems including nonlinear elements is important to assess the impact of such elements on system overvoltages. Real-time transient simulation is necessary for the design and testing of protective relays and controllers in power systems. Representative scenarios of nonlinear behavior in power systems include magnetic saturation, ferroresonance, surge arrester transients, power electronic converter switching, and other nonlinear loads in distribution systems. Almost all of the available offline nonlinear solution algorithms rely on an iterative solution approach, which makes these algorithms computationally expensive compared to the numerical techniques for solving linear systems. For real-time applications, the iterative procedure must be completed within the specified time-step of the transient simulation. Often the nonlinearity is substituted by linear approximations to meet the real-time computation constraint, although at the cost of reduced accuracy of simulation. Therefore, efficient solution algorithms with superior convergence and high accuracy for simulating nonlinear elements in real-time are required.

Manuscript received October 23, 2009; revised November 09, 2009 and April 07, 2010; accepted August 07, 2010. Date of publication September 13, 2010; date of current version April 22, 2011. This work was supported by the Natural Sciences and Engineering Research Council of Canada (NSERC). Paper no. TPWRS-00839-2009.

The authors are with the Department of Electrical and Computer Engineering, University of Alberta, Edmonton, AB T6G 2V4, Canada (e-mail: basghari@ece.ualberta.ca).

Color versions of one or more of the figures in this paper are available online at <http://ieeexplore.ieee.org>.

Digital Object Identifier 10.1109/TPWRS.2010.2066992

The Newton-Raphson (N-R) method is also widely used in the offline simulation of nonlinear systems due to its quadratic convergence. Techniques such as the Compensation Method and the Network Equivalent's Method [1] are implemented in EMT-type programs to improve the efficiency of the N-R algorithm by separating the linear part of the network from the nonlinear part. In traditional EMT-type programs such as ATP, intentional time-step delays were introduced to break nonlinear feedback loops in auxiliary subroutines such as TACS [2]. These delays may cause instability or deteriorate simulation accuracy depending on the length of the time-step and characteristics of the nonlinear system. In [3], an N-R formulation is used for the simultaneous solution of control system nonlinear equations in EMT-type programs.

A variety of relaxation techniques [4], [5] can also be applied to improve the convergence and reduce the number of iterations of the N-R method. However, one of the main limitations of these methods for handling multiple nonlinear elements is that a simultaneous solution of the whole or at least the nonlinear equations of the system is required at each iteration. Therefore, at each iteration, a new linear system with an updated Jacobian matrix must be solved, requiring a large computational effort. Also the choice of initial conditions has a great impact on the convergence of the N-R method to the correct solution, and on the speed of the simulation.

The transmission line modeling (TLM) method was originally developed by Johns and O'Brien [6] as an alternative technique for the time domain simulation of lumped networks containing both linear and nonlinear elements. Later on, its application was extended to the solution of linear integro-differential equations [7] and power electronic circuits [8]. More recently, the TLM technique has been used to solve finite element problems in [9] and [10]. The main advantage of using the TLM for the solution of nonlinear networks is that it effectively decouples the nonlinear elements from each other as well as from the linear part of the network. The decoupling is achieved by connecting the nonlinear elements through lossless lines to the network. The delay time introduced by the lines allows an individual solution using the scalar N-R method, rather than a simultaneous solution of the nonlinear equations using the vector N-R method. This is especially useful in real-time simulation because the solution of individual nonlinear elements can be obtained much faster than the simultaneous solution of the whole equation set [11]. The travel time of the TLM lines does not affect simulation accuracy because the nonlinear equations are solved in the middle of each time-step, and a global simultaneous network solution with a constant admittance matrix is obtained at each time-step. Therefore, the TLM approach is conceptually different from the

methods based on intentional time-step delays between nonlinear elements and other parts of the system. Furthermore, it is proven that the discrete formulation resulting from the TLM method is mathematically equivalent to the Trapezoidal scheme which makes the TLM model unconditionally stable [12].

In this paper, an optimized TLM technique for the real-time transient simulation of circuits with multiple nonlinearities is proposed. In this method, the individual nonlinear equations are solved using a modified scalar N-R iteration based on the golden section method [13], which minimizes the residual of the equations within an iteration. It is shown that through the combination of the TLM method and the modified scalar N-R method, larger time-steps can be adopted for transient simulation without losing accuracy of the solution. Therefore, the proposed approach allows a true nonlinear solution in real-time, whereas the existing commercial EMT-type simulators (either real-time or offline) utilize a non-iterative pseudo-nonlinear solution for the fundamental reason of excessive computational burden. Offline comparison of the proposed method and three other nonlinear solution algorithms, in terms of the CPU time and the accuracy of the simulation, is presented for the case of a nonlinear bridge circuit. The optimized method is then implemented in real-time and real-time oscilloscope results are verified against the experimental measurements of the bridge circuit for two types of loads. A second case study involving the application of surge arresters in a power system is also simulated in real-time.

The paper is organized as follows: Section II gives the background on the vector N-R method and the TLM modeling for linear reactive and nonlinear resistive elements. The proposed optimized TLM method based on the golden section search algorithm is described in Section III. Offline and real-time simulation results and the experimental measurements for a nonlinear diode bridge are presented in Section IV. Section V presents the second case study of a transmission system with multiple surge arresters, followed by the conclusion in Section VI.

II. BACKGROUND

A. Vector N-R Method

The vector N-R solution of a nonlinear circuit involves the simultaneous solution of all circuit equations in an iterative manner. In this paper, this method is distinguished from the scalar N-R method which is applied to individual nonlinear equations only. In order to apply the vector N-R method, the nodal equations of a nonlinear circuit should be written in the form of

$$\mathbf{f}(\mathbf{x}) = \mathbf{0}, \quad (1)$$

where \mathbf{x} is the $(N \times 1)$ vector of unknown nodal voltages.

Then, the first-order Taylor series of nonlinear functions \mathbf{f} is used to obtain the updated solution as follows:

$$\mathbf{f}(\mathbf{x}^{k+1}) \approx \mathbf{f}(\mathbf{x}^k) + \left[\frac{\partial \mathbf{f}^T}{\partial \mathbf{x}} \right]^k (\mathbf{x}^{k+1} - \mathbf{x}^k) = \mathbf{0} \quad (2)$$

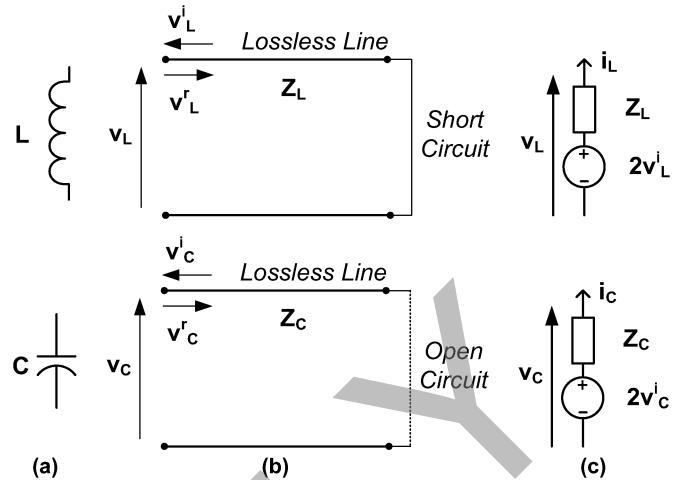


Fig. 1. (a) Linear element. (b) TLM model. (c) Thévenin equivalent.

where \mathbf{x}^{k+1} , $\mathbf{f}(\mathbf{x}^{k+1})$, \mathbf{x}^k , and $\mathbf{f}(\mathbf{x}^k)$ are the solution and residual vector in the $(k+1)$ th and k th iteration, respectively. $[\partial \mathbf{f}^T / \partial \mathbf{x}]^k$ is the $(N \times N)$ Jacobian matrix of the nonlinear system in the k th iteration.

Therefore, the vector N-R method reduces the nonlinear (1) to a system of linear equations in each iteration which can be solved using any linear solution algorithms. The iteration terminates when the magnitude of the incremental vector ($\Delta \mathbf{x}^k = \mathbf{x}^{k+1} - \mathbf{x}^k$) becomes zero within a specified tolerance, or a pre-specified maximum number of iterations is reached. For transient simulation of a nonlinear circuit, a suitable numerical integration technique such as the Trapezoidal Rule should be used to discretize the temporal derivatives prior to applying the vector N-R method.

B. TLM Method

The TLM technique can be used for replacing linear reactive elements with their equivalent discrete models in time, as well as for solving the nonlinear circuit equations within each time-step of the transient simulation.

1) *TLM Models for Linear Reactive Elements:* The surge or characteristic impedance of a lossless transmission line is given as $Z_0 = \sqrt{L/C}$. Depending on the values of L and C , the line can be made predominantly inductive or capacitive.

A linear inductor (L) is modeled as a short-circuited lossless line with the surge impedance $Z_L = 2L/\Delta t$, where $\Delta t/2$ is the one-way travel time of the voltage or current waves on the line. Similarly, a linear capacitor (C) is modeled as an open-circuited lossless line with the surge impedance $Z_C = \Delta t/2C$. These models are obtained from the DC behavior of a line with the same termination.

TLM models and their Thévenin equivalents for a linear inductor and a linear capacitor are shown in Fig. 1. From the Thévenin equivalent of an inductor, the voltage across the inductor at the n th time-step is given as

$${}_n v_L = Z_L \cdot {}_n i_L + 2 \cdot {}_n v_L^i \quad (3)$$

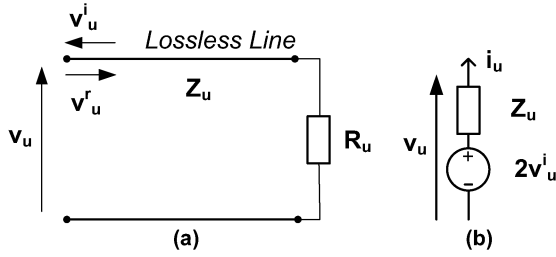


Fig. 2. (a) Nonlinear element TLM model. (b) Thévenin equivalent.

where $n v_L^i$ is the incident voltage pulse and $n i_L$ is the inductor current, at the n th time-step. According to transmission line theory, the voltage across the inductor ($n v_L$) is also equal to the sum of the incident pulse $n v_L^i$ and the reflected pulse $n v_L^r$, i.e.,

$$n v_L = n v_L^i + n v_L^r. \quad (4)$$

For the short-circuit at the far end, the reflection coefficient is -1 . Thus, the reflected pulse $n v_L^r$ will become inverted and act as the incident pulse for the next time-step, i.e.,

$$n+1 v_L^i = -n v_L^r = n v_L^i - n v_L. \quad (5)$$

Based on Fig. 1, similar voltage equations can be developed for a linear capacitor. However, for a capacitor, the reflection coefficient is 1, because the far end is open-circuit. Therefore, the incident pulse for the next time-step is obtained from

$$n+1 v_C^i = +n v_C^r = n v_C - n v_C^i. \quad (6)$$

It can be shown that the TLM capacitor model has a small associated inductance of $L_C = \Delta t^2/4C$ and that the TLM inductor model has a small associated capacitance of $C_L = \Delta t^2/4L$. A physical interpretation of these errors can be derived by recognizing that real inductors do have stray capacitances and that real capacitors also have stray inductances. The parasitic components introduced by the TLM models are similar to stray components in real inductors and capacitors.

2) *TLM Model for Nonlinear Elements*: Fig. 2(a) shows a nonlinear resistor R_u connected by a lossless line, with the surge impedance Z_u and one-way travel time $\Delta t/2$, to the rest of the network. Its Thévenin equivalent is also shown in Fig. 2(b), where the voltage source depends on twice the incident voltage which is the open circuit voltage at the sending end of the line. At the n th iteration, the network launches a pulse $n v_u^r$ into the link, which becomes an incident pulse on the nonlinear resistor at $\Delta t/2$. A reflected pulse produced by the nonlinear element becomes the next incident pulse $n+1 v_u^i$ on the network at Δt . Let the nonlinear resistor be defined from a relationship between its voltage and current, as follows:

$$i_u = f_u(v_u). \quad (7)$$

Once again, using transmission line theory and (7), the following equation can be written at the sending end of the link:

$$\frac{n v_u^r - n+1 v_u^i}{Z_u} = f_u(n v_u^r + n+1 v_u^i). \quad (8)$$

Equation (8) is a single nonlinear equation which can be solved independently by a scalar N-R method to obtain the new incident pulse ($n+1 v_u^i$). Similar equations can be developed for other nonlinear elements in the network.

Although the choice of the surge impedance Z_u is arbitrary, its value influences the speed of convergence. It should be chosen close to the final value of R_u at convergence in order to reduce the transient caused by the mismatch of the TLM line. Of course, since this matched value is not known *a priori*, reflections or iterations must continue until convergence to the final solution.

C. TLM Network Solution

Consider a general electrical circuit \mathcal{N} to which linear reactive elements and nonlinear elements are connected externally. Each of these groups of elements are represented using TLM models, as previously described. The TLM procedure operates by transmitting pulses along the transmission lines. During the delay introduced by the lines, the pulses remain constant. Therefore, the overall model is discrete in time.

At time $t = 0$, the sources will inject pulses out of the ports of \mathcal{N} . These pulses will travel along the lines, be reflected and travel back towards \mathcal{N} . At time $t = \Delta t$, the pulses will be incident upon \mathcal{N} and will scatter into all the ports of \mathcal{N} . These reflected pulses together with new injections from the sources are again launched into the lines and the process repeats. To maintain synchronism, all lines are assumed to have the same round-trip travel time Δt .

Let the incident and reflected pulses at time $t = \Delta t$ be given as

$$n \mathbf{v}^i = [n v_1^i \ n v_2^i \ \dots \ n v_k^i]^T \quad (9)$$

$$n \mathbf{v}^r = [n v_1^r \ n v_2^r \ \dots \ n v_k^r]^T. \quad (10)$$

The network solution in terms of the nodal voltages $n \mathbf{v}$ at the n th time-step is obtained by solving

$$n \mathbf{v} = \mathbf{Y}_n^{-1} \mathcal{I} \quad (11)$$

where \mathbf{Y} and $n \mathcal{I}$ are the nodal admittance matrix and the equivalent nodal source vector of the network at the n th time-step, respectively.

Then, the reflected pulses are calculated from the fact that the sum of the incident and reflected voltage pulses at a node must equal the nodal voltage. Thus

$$n \mathbf{v}^r = \mathbf{A}_n \mathbf{v} - n \mathbf{v}^i \quad (12)$$

where \mathbf{A} is the reduced incident matrix.

The reflected pulses now travel back on the lines and the new incident waves for the next step are obtained from the individual solutions of (5), (6), and (8) for different elements.

If there are multiple nonlinear elements connected to the network, the TLM procedure advances to the next time-step only when the individual solutions for all nonlinear elements have converged in order to maintain synchronism. For a vector N-R solution, \mathbf{Y}^{-1} in (11) must be calculated at every iteration. However, in the TLM solution, \mathbf{Y} remains constant for all

iterations since its entries are only dependent on the surge impedances of the line sections and other linear elements of the network; hence, a unique inversion of \mathbf{Y} is required only at the beginning of the simulation.

D. TLM Iterations

In the applications of the TLM technique to solve nonlinear electromagnetic problems, iterations are usually carried out at both the local and global levels [9], [10]. The local iteration is based on the scalar N-R method to obtain the solution of the individual nonlinear equations. The global iteration consists of repetitively solving (11) due to the mismatch of surge impedances of the TLM lines. Therefore, two different convergence criteria should be defined for the local and global levels. Typically, the local convergence criterion is set to be less strict than the global one to speed up the solution process [14]. On the other hand, when applying the TLM method to nonlinear circuit simulation, it is possible to exclude the global iteration by using a strict convergence criterion for the decoupled individual equations [15]. In this way, the global system of (11) is only solved once in each time-step. Once the convergence is reached for all individual nonlinear equations, the simulation proceeds to the next time-step. The optimized TLM algorithm which is described in the next section is based on a single iteration of the global equation. Nevertheless, the numerical results of both single and multiple iterations in the global level are presented later for the purpose of comparison.

III. OPTIMIZED TLM ALGORITHM

Once the equations of the nonlinear elements are decoupled from each other and the rest of the network by applying the TLM method, it is necessary to use a proper nonlinear solution algorithm for the individual equations. Up to now, the scalar N-R algorithm is usually used for the solution of decoupled nonlinear equations [9], [10], [15]. In this method, the solution of the k th nonlinear equation in the n th iteration can be written as

$${}_n x^k = {}_{n-1} x^k - ({}_{n-1} J^k)^{-1} \cdot f({}_{n-1} x^k) \quad (13)$$

where x is the solution, J is the Jacobian, and f is the residual of the k th nonlinear equation.

However, if the initial guess is not sufficiently close to the solution, the Newton iteration may converge at a slow rate, oscillate, or even diverge for some nonlinear elements. The slow convergence rate results in an excessive number of iterations and CPU time. In circuit simulation, this slow convergence rate usually happens when the nonlinear characteristic of elements has a fast and monotonic derivative (e.g., diodes) [16].

To avoid convergence problems and reduce the number of local iterations, an independent relaxation factor can be applied to each of the scalar N-R solution of the individual nonlinear equations. Therefore, in the optimized TLM method, (13) is modified as follows:

$${}_n x^k = {}_{n-1} x^k - {}_n \alpha_{opt}^k \cdot ({}_{n-1} J^k)^{-1} \cdot f({}_{n-1} x^k) \quad (14)$$

where α_{opt} is the relaxation factor for the k th nonlinear equation in the n th iteration.

The value of the relaxation factor for each element is determined by performing a one-dimensional optimization along the Newton update direction of that element. The objective of this optimization is to find a relaxation factor which minimizes the absolute value of the residual ($|f|$) of the nonlinear equation in each iteration. While different types of optimization techniques can be used to find the relaxation factor, the golden section method [17], which is a kind of linear search method, is superior from the standpoint of the CPU time and the number of function evaluations. The method works by defining four points

$$\alpha_{min} < \alpha_1 < \alpha_2 < \alpha_{max} \quad (15)$$

which satisfy the following conditions:

$$\begin{aligned} |f(\alpha_1)| &\leq |f(\alpha_{min})|, & |f(\alpha_1)| &\leq |f(\alpha_{max})| \\ |f(\alpha_2)| &\leq |f(\alpha_{min})|, & |f(\alpha_2)| &\leq |f(\alpha_{max})|. \end{aligned} \quad (16)$$

α_{min} and α_{max} are arbitrary positive numbers defining the search interval. The above conditions ensure that a minimum of $|f|$ lies in the interval between α_{min} and α_{max} . α_1 and α_2 are given as

$$\alpha_1 = c\alpha_{min} + (1-c)\alpha_{max}, \quad \alpha_2 = (1-c)\alpha_{min} + c\alpha_{max} \quad (17)$$

where $c = ((-1 + \sqrt{5})/2) \approx 0.61803$.

Then, the function $|f|$ is evaluated at α_1 and α_2 . If $|f(\alpha_1)| < |f(\alpha_2)|$, the new search parameters are calculated as follows:

$$\begin{aligned} \alpha_{max}^{new} &= \alpha_2, & \alpha_2^{new} &= \alpha_1 \\ \alpha_{min}^{new} &= \alpha_{min}, & \alpha_1^{new} &= c\alpha_{min} + (1-c)\alpha_2. \end{aligned} \quad (18)$$

If $|f(\alpha_1)| > |f(\alpha_2)|$, the new search parameters are given as

$$\begin{aligned} \alpha_{max}^{new} &= \alpha_{max}, & \alpha_1^{new} &= \alpha_2 \\ \alpha_{min}^{new} &= \alpha_1, & \alpha_2^{new} &= (1-c)\alpha_1 + c\alpha_{max}. \end{aligned} \quad (19)$$

Either way, the width of the bracketing interval will diminish and the location of the minimum of $|f|$ will be better defined. The searching procedure stops when the size of the bracketing interval becomes less than a specified tolerance, and then α_1 or α_2 is substituted in (14) as ${}_n \alpha_{opt}^k$. The flowchart of the search method is shown in Fig. 3. It can be shown that a constant optimal reduction factor of c in the size of the search interval is guaranteed by the golden section search method.

The golden section method is already used in the vector N-R solution of nonlinear equations. In that case, usually a single relaxation factor is applied to all directions of the incremental vector to minimize the L_2 norm of the residual vector [4]. However, as will be shown later, the optimized values of the relaxation factors for different nonlinear elements may vary from each other considerably. The decoupling property of the TLM method provides a convenient way to perform optimization on individual equations. In this manner, the full power of the golden

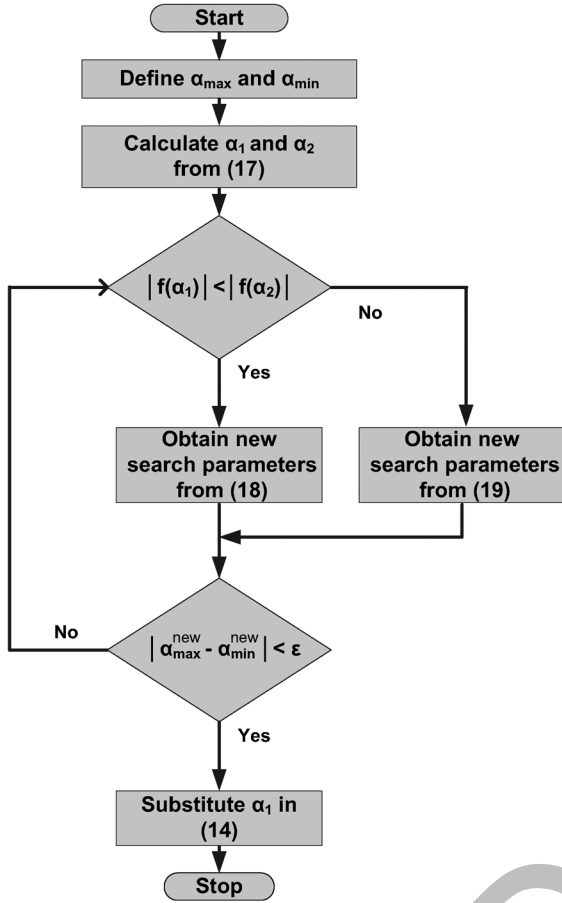
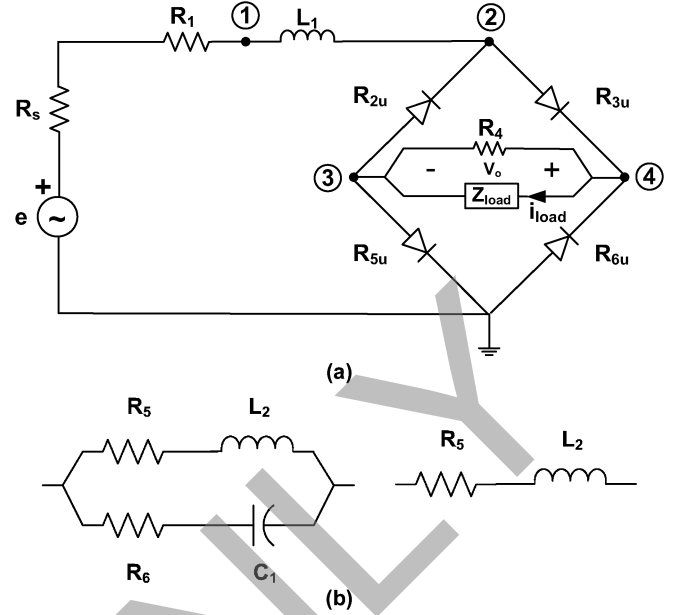


Fig. 3. Flowchart of the golden section search method.

section method can be exploited to reduce the number of iterations. Also the bracketing interval of the golden section search can be chosen in a way to allow both underrelaxation ($\alpha < 1$) and overrelaxation ($\alpha > 1$) factors in the optimization. This is simply achieved by defining the value of α_{\max} higher than 1. It is later shown that the optimized value of α for some nonlinear elements may be located in the overrelaxation region during the transient simulation while for the other elements underrelaxation factors are required.

IV. CASE STUDY I—NONLINEAR BRIDGE

To compare the performance of the above methods, a nonlinear bridge circuit, shown in Fig. 4(a), is used as a case study. The circuit contains four diodes, which are considered as nonlinear resistors (R_{ku} , $k = 2, 3, 5, 6$), three linear resistors (R_s , R_1 and R_4), one linear inductor L_1 , one independent voltage source $e(t)$, and a load Z_{load} . The diodes are characterized by the equation $i_u = I_s [e^{v_u/V_T} - 1]$. With such characteristics, the operation of the bridge is similar to that of a full-wave diode rectifier. Two kinds of loads (Z_{load}), i.e., resistive-inductive (RL) and resistive-inductive-capacitive (RLC), are considered for the simulation, as shown in Fig. 4(b). The numerical values of the circuit parameters are given in Table III in the Appendix.


 Fig. 4. (a) Nonlinear diode bridge. (b) Z_{load} .

A. Vector N-R Solution

The vector N-R problem is to find $\mathbf{X} \in \mathbb{R}^3$ such that

$$\mathbf{f}(\mathbf{x}) = 0, \quad \mathbf{f} : \mathbb{R}^3 \mapsto \mathbb{R}^3 \quad (20)$$

where $\mathbf{x} = [v_2 \ v_3 \ v_4]^T$ and $\mathbf{f} = [f_2 \ f_3 \ f_4]^T$.

In the case of the RL load, the nonlinear nodal equations of the bridge are obtained by replacing the series RL elements with their discrete equivalents using the Trapezoidal method. In this way, only three independent nodes (2, 3, and 4) remain in the circuit. Then, KCL is applied to each independent node to obtain

$$f_2 = I_s \left(e^{\frac{v_3(t) - v_2(t)}{V_T}} - 1 \right) - I_s \left(e^{\frac{v_2(t) - v_4(t)}{V_T}} - 1 \right) + A_1 (e(t) - v_2(t)) + A_2 I_{hL1}(t - \Delta t) \quad (21)$$

$$f_3 = -R_4 I_s \left(e^{\frac{v_3(t) - v_2(t)}{V_T}} - 1 \right) - R_4 I_s \left(e^{\frac{v_3(t)}{V_T}} - 1 \right) + (v_4(t) - v_3(t)) - R_4 A_3 (v_3(t) - v_4(t)) - R_4 I_{hL2}(t - \Delta t) \quad (22)$$

$$f_4 = R_4 I_s \left(e^{\frac{v_2(t) - v_4(t)}{V_T}} - 1 \right) + R_4 I_s \left(e^{\frac{-v_4(t)}{V_T}} - 1 \right) - (v_4(t) - v_3(t)) + R_4 A_3 (v_3(t) - v_4(t)) + R_4 I_{hL2}(t - \Delta t) \quad (23)$$

where A_1 , A_2 , and A_3 are constant coefficients. I_{hL1} and I_{hL2} are history currents sources.

For the simulation of the RLC load [Fig. 4(b)], discrete equivalent of the RC branch is also included in the nodal equations of f_3 and f_4 .

The solution of (20) is given as

$$\mathbf{x}^{k+1} = \mathbf{x}^k - \alpha \mathbf{J}^{-1} \mathbf{f}(\mathbf{x}^k) \quad (24)$$

where \mathbf{J} and α are the Jacobian matrix and the relaxation factor, respectively.

The convergence criteria for the vector N-R iteration is defined as

$$\|\mathbf{x}^{k+1} - \mathbf{x}^k\| < \varepsilon_x \text{ and } \|\mathbf{f}(\mathbf{x}^{k+1})\| < \varepsilon_f \quad (25)$$

with ε_x and ε_f set at 10^{-5} . Maximum number of iterations for the vector N-R solution is limited to 30.

B. TLM Solution With Scalar N-R

For the RL load, five nodal voltages are considered as the variables of the circuit. The nodes include four external ones as shown in Fig. 4 and one internal node (node 5) between the resistor and inductor of the load. The TLM model for the nonlinear bridge is obtained by first replacing the voltage source (e) and series resistors ($R_s + R_1$) by a Norton equivalent. Then L_1 , R_{ku} ($k = 2, 3, 5, 6$), and the load inductor L_2 are substituted by their individual transmission line sections and subsequently by their Norton equivalents. The characteristic impedances for the lines are Z_{L1} and Z_{L2} for the inductors, and Z_{ku} ($k = 2, 3, 5, 6$) for the diodes. At each time-step the TLM solution executes (11) and (12), where

$$n\mathbf{v}^i = [n v_{L1}^i \ n v_{2u}^i \ n v_{3u}^i \ n v_{5u}^i \ n v_{6u}^i \ n v_{L2}^i]^T \quad (26)$$

$$\mathbf{I} = \begin{bmatrix} \frac{e(t)}{(R_s + R_1)} - \frac{2v_{L1}^i}{Z_{L1}} \\ \frac{2v_{L1}^i}{Z_{L1}} - \frac{2v_{2u}^i}{Z_{2u}} - \frac{2v_{3u}^i}{Z_{3u}} \\ \frac{2v_{2u}^i}{Z_{2u}} - \frac{2v_{3u}^i}{Z_{3u}} \\ \frac{2v_{3u}^i}{Z_{3u}} - \frac{2v_{6u}^i}{Z_{6u}} - \frac{2v_{L2}^i}{Z_{L2}} \\ \frac{2v_{L2}^i}{Z_{L2}} \end{bmatrix}. \quad (27)$$

In addition, within every time-step, the new incident pulses $n_{+1}v_{ku}^i$, ($k = 2, 3, 5, 6$) are obtained by solving the following equations of the nonlinear resistors (diodes) independently:

$$n v_{ku}^r - n_{+1} v_{ku}^i = \pm Z_{ku} I_s \left(e^{\pm \frac{(n v_{ku}^r + n_{+1} v_{ku}^i)}{V_T}} - 1 \right). \quad (28)$$

Three different schemes for the TLM solution are implemented and compared with each other, as follows:

- 1) **TLM solution with multiple global iterations:** In this scheme, the global system of nodal (11) is solved several times within each time-step until the convergence is achieved or the number of iterations reaches its maximum allowed value. The global convergence criterion is defined as

$$\|\mathbf{x}^{k+1} - \mathbf{x}^k\| < 10^{-5}. \quad (29)$$

In this scheme, the individual local nonlinear equations are solved by the scalar N-R method and the convergence criterion for local equations are set to be the same as the global one (e.g., 10^{-5}).

- 2) **TLM solution with a single global iteration:** In this scheme, the global system of nodal (11) is solved only once within each time-step. The individual local nonlinear

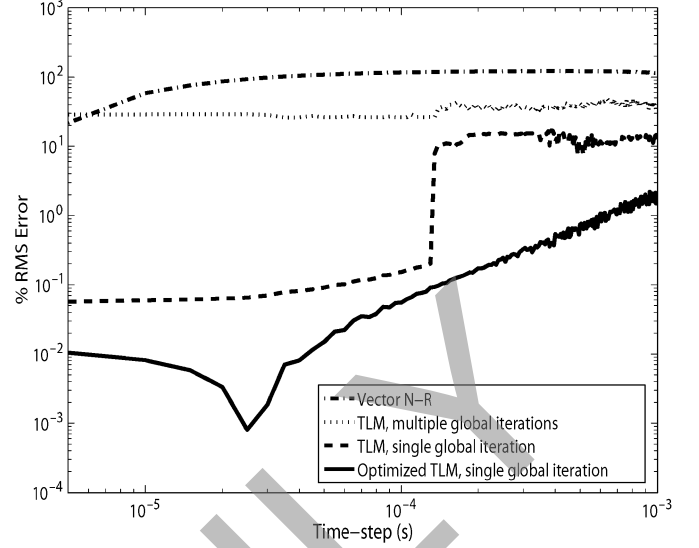


Fig. 5. Percentage RMS error in v_o for different nonlinear solution methods (RL load).

equations are solved by the scalar N-R method and the convergence criterion for local equations is set to be

$$|x_i^{k+1} - x_i^k| < 10^{-5} \quad i = 1, 2, 3, 4. \quad (30)$$

- 3) **Optimized TLM solution with a single global iteration:**

In this scheme, the global system of nodal (11) is solved only once within each time-step. The individual local nonlinear equations are solved by the relaxed N-R method. The value of the relaxation factor for each nonlinear equation is obtained by performing a golden section search algorithm, as already described. The convergence criterion for local equations are set to be

$$|x_i^{k+1} - x_i^k| < 10^{-5} \quad i = 1, 2, 3, 4. \quad (31)$$

The same formulation is also used for the RLC load, except that in that case, an extra internal node is defined between the series resistor and capacitor, and the TLM model of the capacitor is also included in the circuit equations.

C. Offline Comparison

The offline simulation of the nonlinear bridge by the use of the vector N-R and the TLM algorithms was carried out for different time steps. A comparison of the results is then made based on the criteria of convergence (number of iterations), accuracy (RMS error) and CPU time requirement. All methods were coded in MATLAB and executed on a Pentium 4 2.8-GHz processor. Under AC steady-state conditions, Figs. 5 and 6 show the percentage RMS error in the output voltage ($v_o = v_4 - v_3$) and CPU time, for a simulation of 0.09 s of the RL load. All methods start from zero initial conditions with the cosine excitation of the voltage source. The simulation time-step Δt is varied from $5 \mu\text{s}$ to $1000 \mu\text{s}$.

To avoid the convergence problem in the vector N-R method, a constant underrelaxation factor of 0.1 is applied to the solution. However, as can be seen in Figs. 5 and 6, the vector N-R

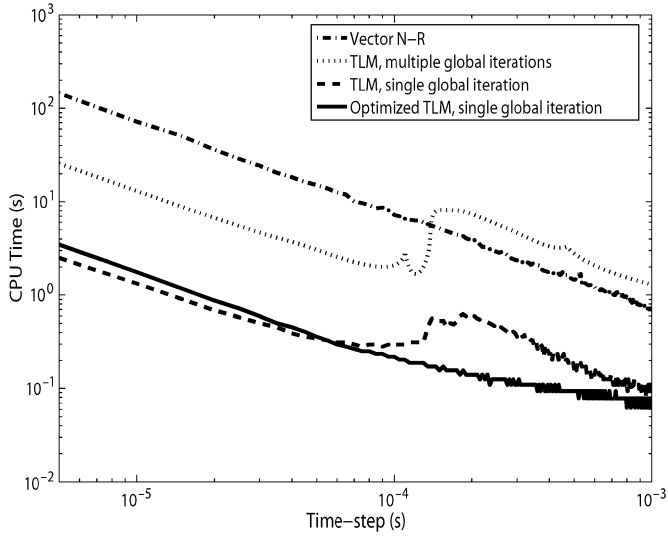


Fig. 6. CPU execution time for different nonlinear solution methods (RL load).

simulation results show a relatively large and constant steady-state error (around 100%) in the output voltage and also need a large CPU time to complete the simulation for all time steps. This is mainly due to the sensitivity of the vector N-R method to the initial conditions. For a cosine excitation, the zero initial condition is far from the solution; therefore the vector N-R method converges to a wrong solution (or even diverges) in both transient and steady-state conditions. A large and constant steady-state error of about 30% is also present in the simulation result for the TLM with multiple global iterations.

On the other hand, no convergence problem occurs with any of the two TLM methods with a single global iteration for different time-steps. It is also found that the number of N-R iterations in the optimized method is always less than that of the other TLM methods. From Figs. 5 and 6, it can be seen that for small time-steps, the TLM with a single global iteration is superior in terms of the CPU time while its error is slightly higher than that of the optimized TLM method. Therefore, the time requirement for performing the golden section search method exceeds the time-saving from the reduction in the number of iterations for small time-steps. However, as the time-step of the simulation is increased, at a certain point ($\Delta t = 130 \mu\text{s}$ in this case) the TLM method with a single global iteration begins to take more CPU time than that of the optimized TLM method, and its error also drastically increases over 10%. This is while the maximum error of the optimized method is 2% for the RL load for all time-steps. The large difference in the error of the two methods can be seen from Fig. 5. Similar results are also observed for the bridge with the RLC load. It can be concluded from the simulation result that the optimized TLM method with a single global iteration has the best performance in terms of the accuracy and simulation time among the different nonlinear solution algorithms for both small and large time-steps.

Fig. 7 shows the optimized relaxation factors for R_{2u} (diode 1) and R_{3u} (diode 2) during the first iteration in each time-step of the transient simulation with the time-step of $\Delta t = 300 \mu\text{s}$. As can be seen, although both relaxation factors follow a similar pattern due to the symmetry of the circuit, their instanta-

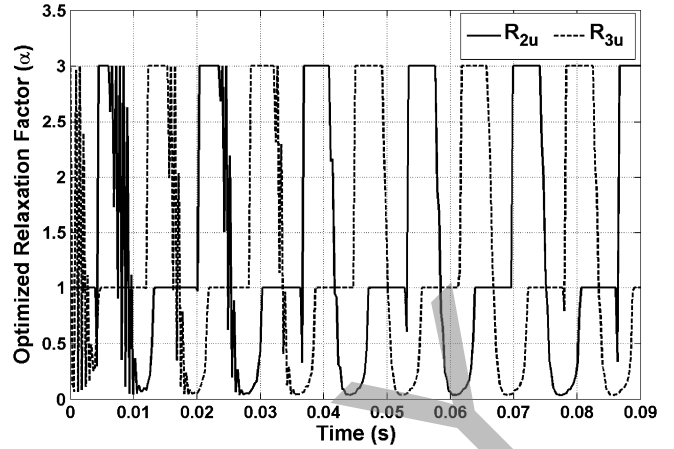


Fig. 7. Optimized relaxation factors for R_{2u} and R_{3u} during the transient simulation of the RL load.

neous values differ from each other considerably. Therefore, it is necessary to perform the optimization on each decoupled equation separately. Also it is obvious that the optimized value of α may be located in underrelaxation or overrelaxation regions depending on the instant of simulation. The maximum value of the overrelaxation factor is limited to 3 for the nonlinear bridge due to the risk of instability with larger relaxation factors.

Simulation results show that the value of optimized relaxation factor normally becomes very close to 1 after the first or second iteration due to the proximity to the final solution when no relaxation factor is required for the remaining iterations. Therefore, without losing the generality of the proposed approach, the golden section method can be applied to only the first two iterations of each nonlinear equation. This simplifying assumption is not used here to have a general and unconditional comparison of the proposed method with other nonlinear algorithms.

Based on the simulation results given above, it is concluded that the optimized TLM method with a single global iteration provides more flexibility in selecting larger time-steps for the simulation, and therefore, it is the best option for real-time applications.

D. Real-Time Simulation

To obtain the time-domain simulation results of the nonlinear bridge, the optimized TLM method was coded in the C language and embedded as a dynamically linked program (S-function) in the MATLAB/SIMULINK environment. The real-time simulation of the bridge was carried out on one target node of a PC-cluster-based real-time simulator [18] using a distributed real-time software package known as RT-LAB [19]. The target processor is a 3.0-GHz Intel Xeon. Real-time simulation results are observed through an oscilloscope connected to the I/O terminals of the target node. To include the voltage source distortion in the simulation, the supply voltage of the experimental setup was sampled and used as the input in the real-time simulation. All the real-time simulations are performed using a time-step of $\Delta t = 40 \mu\text{s}$.

Fig. 8(a) shows the transient responses of the input (e) and output (V_o) voltages and the load current (i_{load}) as defined in Fig. 4 for the RL load. As can be seen, the rectified output

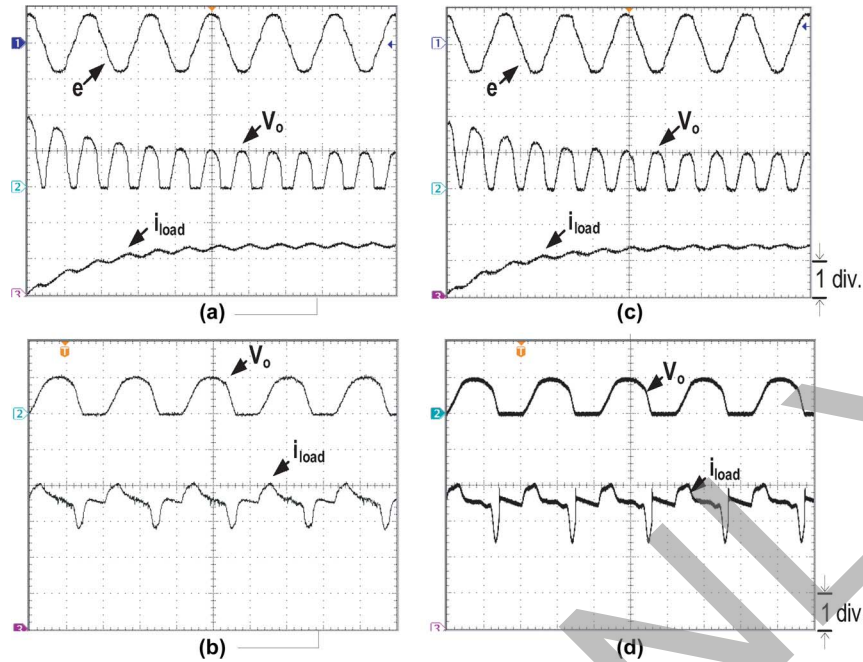


Fig. 8. (a) Real-time results for e (200 V/div.), V_o (50 V/div.), and i_{load} (0.33 A/div.) for the RL load with a $40 \mu s$ time-step of, x-axis: 0.01 s/div. (b) Real-time results for V_o (50 V/div.), and i_{load} (0.133 A/div.) for the RLC load with a $40 \mu s$ time-step, x-axis: 0.004 s/div. (c) Experimental results for the RL load. (d) Experimental results for the RLC load.

TABLE I
FREQUENCY COMPONENTS OF THE OUTPUT VOLTAGE
AND THE LOAD CURRENT FOR CASE STUDY I

f (Hz)	RL Load		RLC Load	
	Real-time (V)	Experiment (V)	Real-time (mA)	Experiment (mA)
DC	20.20	19.20	440	424
120	18.70	18.50	28	30
240	-	-	-	-
360	3.40	3.46	18	17
480	1.00	0.96	-	-
600	1.00	0.95	8.8	9.6

voltage is almost one third of the input voltage due to the large voltage drop across the supply resistor R_1 . Also when the absolute value of the input voltage e is small, the load inductor current closes its path through the upper (lower) diodes of the bridge. This produces a small negative voltage (-2.7 V), which is equal to twice that of a diode voltage drop, across the output terminals. The large load inductor draws a smooth steady-state load current with a DC value of 0.46 A and a small ripple of 0.03 A (peak to peak). The real-time simulation time-step can be increased up to $\Delta t = 1000 \mu s$ while the error remains less than 2% owing to the use of the optimized TLM method.

Fig. 8(b) shows the steady-state responses of the output (V_o) voltage and the load current (i_{load}) for the RLC load. In this case, the output voltage is almost identical to that of the RL load. However, the capacitive branch draws a current which is nearly proportional to the derivative of the output voltage. Therefore, the general shape of the load current waveform is considerably different from that of the RL load with a DC value of 0.44 A and a ripple of 0.16 A (peak to peak).

The execution time for the real-time simulation ($7.162 \mu s$) is less than 18% of the total step-size ($40 \mu s$). This means that a

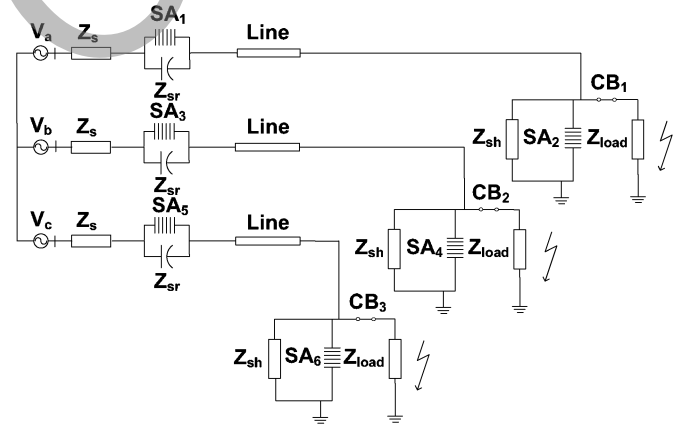


Fig. 9. Transmission system with surge arresters.

large time margin is available to increase the number of non-linear elements in the system and the number of hardware I/Os.

E. Experimental Results

In order to verify the real-time simulation results, an experimental setup of the nonlinear bridge was implemented. Fig. 8(c) and (d) shows the time-domain responses of the RL and RLC loads, respectively, obtained from the experiment. It can be seen that the simulation results are in close agreement with the experiment. For the RL load, the discrepancy between the simulation and measurement is very small for all parameters. In the case of RLC load, the predicted value of the minimum load current (0.373 A) is slightly higher than the measurement (0.320 A). This is mainly due to the large sensitivity of the capacitor current to small variations in the output voltage which requires a very small step size for the simulation. Furthermore, the neglecting of

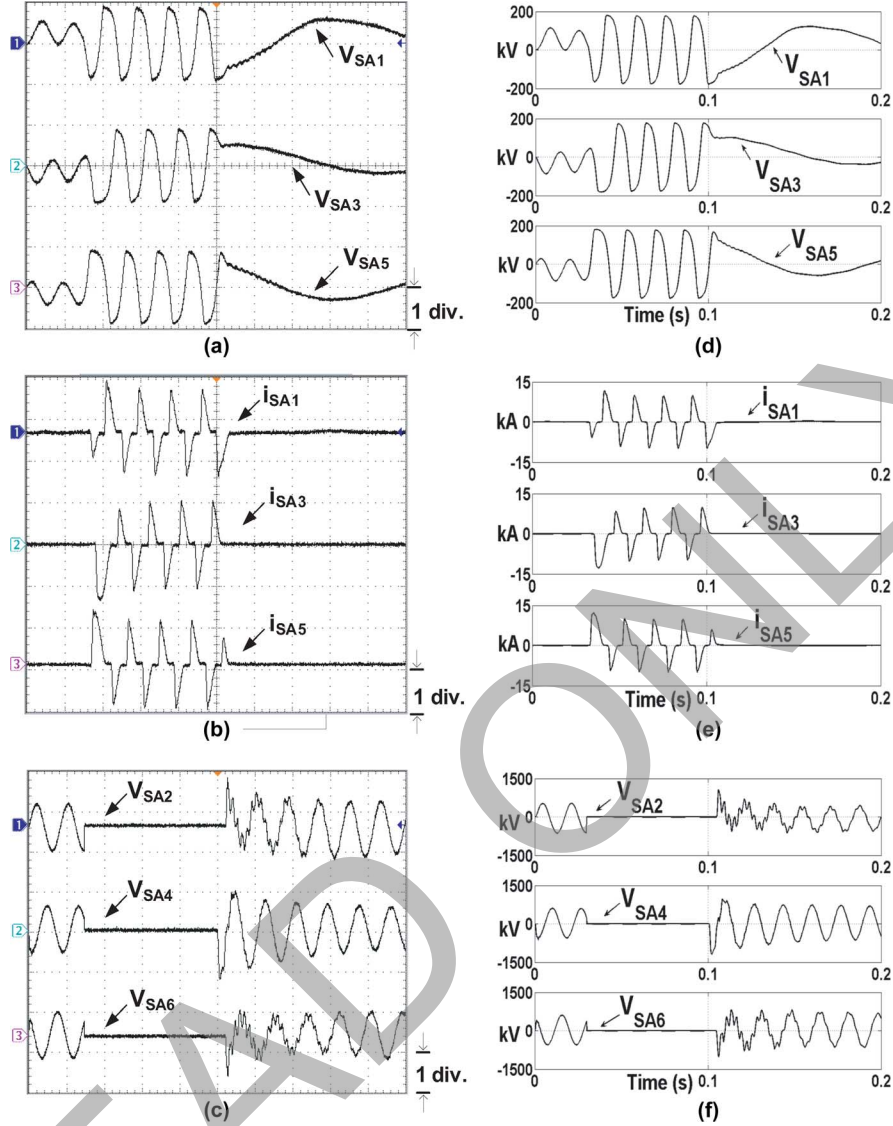


Fig. 10. (a) Real-time transient overvoltages across series capacitors. x-axis: 0.02 s/div, y-axis: 200 kV/div. (b) Real-time transient surge arrester currents. x-axis: 0.01 s/div, y-axis: 10 kA/div. (c) Real-time transient overvoltages across the shunt compensators. x-axis: 0.02 s/div, y-axis: 1000 kV/div. (d), (e), (f) Corresponding offline simulation results.

stray circuit components and the approximate diode model used in the simulation can contribute to small discrepancies. Apart from this, the general shape of the simulated load current and voltage and their numerical values match very closely with the experiment.

For the purpose of comparison, major frequency components of the output voltage (V_o) for the RL load and the load current (i_{load}) for the RLC load, obtained from the real-time simulation and the experiment, are shown in Table I. As can be seen, the frequency components of the real-time simulation and experimental results are very similar to each other. Small discrepancies are observed which are mainly due to the error in the measurement of the circuit parameters used in the simulation. Also the difference between the sampling rate of the oscilloscope and the real-time simulation time-step may result in a small deviation of the frequency components in the simulation results from that of the experimental ones.

V. CASE STUDY II—SURGE ARRESTERS IN A TRANSMISSION NETWORK

This case study consists of a 735-kV transmission system feeding a load through a 100-km transmission line. The line is series compensated at the sending end and shunt compensated at its receiving end. Both series and shunt compensators are protected against overvoltage conditions by using surge arresters. The schematic of the transmission system is shown in Fig. 9.

The physical transmission line in each phase is modeled by the Bergeron line model. The arresters are highly nonlinear resistors characterized by

$$\frac{i}{I_{ref}} = \left(\frac{v}{V_{ref}} \right)^\beta \quad (32)$$

where β is the exponent, I_{ref} and V_{ref} are arbitrary reference values which normalize the equation. In this case study, β , V_{ref}

TABLE II
FREQUENCY COMPONENTS OF RESULTS FOR CASE STUDY II

f (Hz)	V_{SA1}		i_{SA1}		V_{SA2}	
	Real-time (kV)	Off-line (kV)	Real-time (kA)	Off-line (kA)	Real-time (kV)	Off-line (kV)
DC	64.7	64.1	-	-	-	-
60	78.8	79.2	5.45	5.54	562	566
180	8.42	8.44	2.43	2.33	-	-
300	2.05	2.14	0.78	0.74	-	-
420	-	-	0.5	0.53	74.9	72.3
540	-	-	0.36	0.34	-	-
900	-	-	-	-	3.64	3.56

(for SA_1 , SA_3 , and SA_5), V_{ref} (for SA_2 , SA_4 , and SA_6), I_{ref} (for SA_1 , SA_3 , and SA_5), and I_{ref} (for SA_2 , SA_4 , and SA_6) are 9, 185 kV, 1081 kV, 15 kA, and 1 kA, respectively. All the network parameters are listed in Table III in the Appendix. The system is energized at $t_0 = 0$ s, followed by a three-phase fault at the load terminals at $t_1 = 0.03$ s. The fault is cleared by circuit breaker (CB_1 to CB_3) opening at $t_2 = 0.1$ s.

The three-phase power system includes 19 nodal voltages and six nonlinear elements (surge arresters SA_1 to SA_6). The optimized TLM algorithm with a time-step of $\Delta t = 50 \mu s$ is used for real-time simulation of the network.

Fig. 10(a) shows the transient response of voltages across the surge arresters SA_1 , SA_3 , and SA_5 . When the three-phase fault is applied at the load terminals, series capacitor voltages increase resulting in the conduction of arresters in parallel with the capacitors. The arrester conduction limits the maximum overvoltage across the capacitors to 180 kV (peak) compared to 755 kV (peak) without the arresters. Large nonlinear currents are drawn by the arresters during the conduction time, reaching a peak of 12.5 kA in phases A and B, and -13.3 kA in phase C, as shown in Fig. 10(b). Once the fault is cleared, the capacitor voltages slowly damp to a small value because the load is disconnected from the power system. Voltages across the shunt surge arresters SA_2 , SA_4 , and SA_6 are depicted in Fig. 10(c). These voltages are zero during the fault as expected. After the breaker opening, overvoltages at the shunt compensator terminals are limited by the conduction of these arresters to a maximum of -1200 kV in phase B compared to -1930 kV without the arresters.

All of the above real-time results have been verified using an offline SimPowerSystems model in Matlab/Simulink. The time-domain results from the offline model are depicted in Fig. 10(d)–(f) and are similar to the real-time results. The major frequency components of v_{SA1} , i_{SA1} , and v_{SA2} obtained from real-time and offline simulations are given in Table II. The data window of DFT for each signal is adjusted to capture the whole period of the transient.

The optimized TLM algorithm allows pre-computation of network admittance matrix and its inverse, as the nonlinear surge arresters are replaced by their equivalent transmission line sections. This results in a considerable time saving compared to the vector N-R method which requires dynamic inversion of the Jacobian matrix (19×19) during the course of simulation. The optimized TLM method ensures that the minimum number of local iterations are preserved in each time-step with a total

TABLE III
DATA FOR THE CASE STUDIES

Case Study I Parameters	Values
R_s, R_1, R_4, Z_{ku}	$5\Omega, 167.4\Omega, 297\Omega, 100\Omega$
L_1, ω	$1mH, 377rad/s$
$e(t)$	$165 \cos(\omega t)$
I_s, V_T	$3 \times 10^{-4}A, 0.2172V$
Z_{load1}	$(44.2 + j904.8)\Omega$
Z_{load2}	$Z_{load1} \parallel (80.1 - j914.66)\Omega$
Case Study II Parameters	Values
Base values	735kV, 60Hz
Short circuit impedance (Z_s)	$(3.6 + j36)\Omega$
Series compensator impedance (Z_{sr})	$-j26.2\Omega$
Transmission line resistance	$0.01\Omega/km$
Transmission line inductance	$0.87mH/km$
Transmission line capacitance	$13.41nF/km$
Shunt compensator impedance (Z_{sh})	$(8.18 + j1636.93)\Omega$
Load impedance (Z_{load})	270.11Ω
β	9
V_{ref} for SA_1, SA_3 , and SA_5	185kV
V_{ref} for SA_2, SA_4 , and SA_6	1081kV
I_{ref} for SA_1, SA_3 , and SA_5	15kA
I_{ref} for SA_2, SA_4 , and SA_6	1kA

computation time of $30 \mu s$ out of $\Delta t = 50 \mu s$. The large idle time present in each time-step shows the possibility of modeling even larger systems in real-time with more nonlinear elements. The SimPowerSystems model was also tested in real-time; however, a large number of overruns (violation of specified time-step) were observed during the course of simulation. This clearly shows the advantage of using the optimized TLM method for real-time applications.

VI. CONCLUSION

Accurate transient simulation of systems with multiple nonlinearities is challenging in real-time because of the need to perform a simultaneous iterative N-R solution. This paper proposes a method which effectively breaks the problem into individual nonlinear elements using transmission line modeling (TLM). This has the advantage of dealing with the nonlinearities individually using a scalar N-R iterative scheme, thereby increasing computational efficiency. The TLM algorithm is further optimized using the golden section search method. The optimized TLM method allows the simulation to be performed using larger time-steps compared to other nonlinear solution algorithms, while also maintaining the accuracy within reasonable limits. A detailed case study is carried out on a nonlinear diode bridge to show the accuracy and efficiency of the algorithm. Real-time simulation results show close agreement with experimental measurements. A second case study of a transmission system with multiple surge arresters is also simulated in real-time using the optimized TLM method.

APPENDIX

Table III lists the data for the case studies.

REFERENCES

- [1] H. W. Dommel, "Nonlinear and time-varying elements in digital simulation of electromagnetic transients," *IEEE Trans. Power App. Syst.*, vol. PAS-90, pp. 2561–2567, Jun. 1971.
- [2] L. Dubé and H. W. Dommel, "Simulation of control systems in an electromagnetic transients program with TACS," in *Proc. IEEE Power Industry Computer Applications Conf.*, 1977, pp. 266–271.

- [3] J. Mahseredjian, L. Dubé, M. Zou, S. Dennerrière, and G. Joos, "Simultaneous solution of control system equations in EMTP," *IEEE Trans. Power Syst.*, vol. 21, no. 1, pp. 117–124, Feb. 2006.
- [4] T. Nakata, N. Takahashi, K. Fujiwara, N. Okamoto, and K. Muramatsu, "Improvement of convergence characteristics of Newton-Raphson method for nonlinear magnetic field analysis," *IEEE Trans. Magn.*, vol. 28, no. 2, pp. 1048–1051, Mar. 1992.
- [5] K. Fujiwara, T. Nakata, N. Okamoto, and K. Muramatsu, "Method for determining relaxation factor for modified Newton-Raphson method," *IEEE Trans. Magn.*, vol. 29, no. 2, pp. 1962–1965, Mar. 1993.
- [6] P. B. Johns and M. O'Brien, "Use of transmission-line method to solve nonlinear lumped networks," *Radio Electron. Eng.*, vol. 50, no. 1/2, pp. 59–70, Jan. 1980.
- [7] S. Y. R. Hui and C. Christopoulos, "Discrete transform technique for solving coupled integro-differential equations in digital computers," *Proc. Inst. Elect. Eng. A*, vol. 138, no. 5, pp. 273–280, Sep. 1991.
- [8] S. Y. R. Hui and C. Christopoulos, "Modeling nonlinear power electronic circuits with the transmission-line modeling technique," *IEEE Trans. Power Electron.*, vol. 10, no. 1, pp. 48–54, Jan. 1995.
- [9] J. Lobry, J. Trecat, and C. Broche, "The transmission line modeling method as a new iterative technique in nonlinear magnetostatics," *IEEE Trans. Magn.*, vol. 32, no. 2, pp. 559–566, Mar. 1996.
- [10] O. Deblecker, J. Lobry, and C. Broche, "Use of transmission-line modeling method in FEM for solution of nonlinear eddy-current problems," *Proc. Inst. Elect. Eng., Sci., Meas., Technol.*, vol. 145, no. 1, pp. 31–38, Jan. 1998.
- [11] V. Dinavahi, "Modeling and simulation of multiple nonlinearities using TLM," in *Proc. Int. Power System Transients Conf. (IPST 2005)*, Montreal, QC, Canada, Jun. 2005.
- [12] O. Deblecker, J. Lobry, and C. Broche, "Novel algorithm based on transmission-line modeling in the finite-element method for nonlinear quasi-static field analysis," *IEEE Trans. Magn.*, vol. 39, no. 1, pp. 529–538, Jan. 2003.
- [13] R. H. Gallagher and O. C. Zienkiewicz, *Optimum Structural Design—Theory and Applications*. New York: Wiley, 1973.
- [14] R. E. Knight and C. Broche, "Application of domain decomposition and transmission line modelling techniques to 2D, time-domain, finite element problems," *IEEE Trans. Magn.*, vol. 35, no. 3, pp. 1478–1481, May 1999.
- [15] V. Dinavahi, "Transient analysis of systems with multiple nonlinear elements using TLM," *IEEE Trans. Power Syst.*, vol. 13, no. 4, pp. 2102–2103, Nov. 2004.
- [16] E. Ngoya, J. Rousset, and J. Obregon, "Newton-Raphson iteration speed-up algorithm for the solution of nonlinear circuit equations in general-purpose CAD programs," *IEEE Trans. Comput.-Aided Des. Integr. Circuits Syst.*, vol. 16, no. 6, pp. 638–644, Jun. 1997.
- [17] W. H. Press, S. A. Teukolsky, W. T. Vetterling, and B. P. Flannery, *Numerical Recipes in C*. Cambridge, U.K.: Cambridge Univ. Press, 1992.
- [18] L-F. Pak, M. O. Faruque, X. Nie, and V. Dinavahi, "A versatile cluster-based real-time digital simulator for power engineering research," *IEEE Trans. Power Syst.*, vol. 21, no. 2, pp. 455–465, May 2006.
- [19] "RTLAB Version 8.1 User Guide," Opal-RT Technologies Inc., 2007.



Babak Asghari (S'06) received the B.Sc. and M.Sc. degrees in electrical engineering from Sharif University of Technology, Tehran, Iran. Currently, he is pursuing the Ph.D. degree in the Department of Electrical and Computer Engineering at the University of Alberta, Edmonton, AB, Canada.

His research interests include real-time digital simulation and control of power systems and electrical drives.



Venkata Dinavahi (S'94–M'00–SM'08) received the Ph.D. degree in electrical and computer engineering from the University of Toronto, Toronto, ON, Canada, in 2000.

He is a Professor at the University of Alberta, Edmonton, AB, Canada, and his research interests include real-time simulation of power systems and power electronic systems, large-scale system simulation, and parallel and distributed computing.